European Journal of Inorganic Chemistry

Supporting Information

Role of Alkylated 2,6-bis(tetrazol-5-yl)pyridyl Ligands and Iron(II) Salts in Selecting Spin Crossover Complexes

Rita Mazzoni,* Stefano Baratti, Daniel Rustichelli, Stefano Stagni, Valentina Fiorini, Stefano Zacchini, Dawid Pinkowicz, Alessandra Forni, Jasper R. Plaisier, Lara Gigli, and Luca Rigamonti*

SUPPORTING INFORMATION (SI) FOR:

Role of Alkylated 2,6-bis(tetrazol-5-yl)pyridyl Ligands and Iron(II) Salts in Selecting Spin Crossover Complexes

Rita Mazzoni, Stefano Baratti, Daniel Rustichelli, Stefano Stagni, Valentina Fiorini, Stefano Zacchini, Dawid Pinkowicz, Alessandra Forni, Jasper R. Plaisier, Lara Gigli, and Luca Rigamonti

Index

Experimental Section (cont.)

X-ray Crystal Structure Determinations. Single crystals suitable for X-ray diffraction were obtained from slow evaporation of CH_3CN and EtOH for Me_2btp and *t*Bu_2btp, respectively, and from slow diffusion of Et_2O in DCM solutions for **1a**·0.67DCM, **2a**·0.5Et_2O, **2b** and **4a**·4DCM. Crystal data together with data collection and refinement for Me_2btp, *t*Bu_2btp, **1a**·0.67DCM, **2a**·0.5Et_2O, **2b** and **4a**·4DCM are given in Table S1. Intensity data for all compounds were collected on a Bruker Apex II with a Photon100 area detector using graphite monochromatic Mo-$K\alpha$ radiation, except for *t*Bu_2btp, which was analysed by means of a Bruker D8 Quest Eco Photon50 CMOS diffractometer equipped with a Mo-Kα generator (graphite monochromator, λ = 0.71073 Å). The structures were solved by direct methods and refined by full-matrix least-squares based on all data using F^2.[1] Hydrogen atoms were fixed at calculated positions and refined using a riding model, except the H-atoms bonded to the H_2O molecule of **2b**, which were located in the Fourier map and refined isotropically. The crystals of **4a**·4DCM appeared to be non-merohedrally twinned. The TwinRotMat routine of PLATON[2] was used to determine the twinning matrix and to write the reflection data file (.hkl) containing the two twin components. Refinement was performed using the instruction HKLF 5 in SHELXL and one BASF parameter, which refined as 0.256(5).

Computational details. M06/6-311+G(d) gas-phase geometry optimizations were performed on R_2btp ligands and the $[Fe^{II}(R_2btp)_2]^{2+}$ dications, optimizing their geometry in both LS and HS states. All minima were confirmed by frequency calculations. The M06 functional was chosen owing to its ability to correctly describe organometallic complexes.[3] All calculations have been performed with Gaussian 16 program (Revision A.03).[4]

Magnetic measurements. Magnetic measurements on the different solvates of **4a** were performed using a Quantum Design MPMS3 magnetometer equipped with a 7 T magnet. In particular, a polycrystalline sample of **4a**·4DCM was loaded into a gas-tight custom-made delrin sample holder.[5] The temperature dependence of χ_M was monitored from 1.8 to 300 K by applying H_{DC} = 1 kOe, and the magnetic data were corrected for the sample holder contribution and the diamagnetism of the sample calculated from Pascal's constants.[6]

Powder X-ray diffraction experiments. Yellow needle crystals of **4a**·4DCM were grinded to obtain microcrystalline powders and then they were divided into three different fractions: *i*) untreated sample (***solvated***), flame-sealed in a quartz capillary with the mother liquor; *ii*) vacuum-pumped sample for

2 h in order to remove DCM molecules and stored in under argon atmosphere and sealed in a quartz capillary (***dry***) and *iii*) vacuum-pumped sample for 2 h and then exposed to air and sealed in a quartz capillary (***hydrated***). Replicates of the different samples were prepared from two distinct synthetic batches to assure the best data collections. All capillaries were analysed at the Materials Characterisation by X-ray diffraction (MCX)[7] beamline at the Elettra Synchrotron of Trieste with incident wavelength λ = 1.2400 Å, on a 4-circle Huber goniometer equipped with a scintillation detector. Powder samples were loaded and packed in a 0.5 mm quartz capillary, mounted on a standard goniometric head, and spun during data collection. The low temperatures were reached using a Cryojet system at liquid nitrogen of Oxford instruments.

Two different types of measurements were conducted: rapid-scan spectra from 4 to 40° in 2θ, with 0.008° steps and exposure time of 0.5 s for each step without stopping (about 30 minutes for each experiment), and high-resolution spectra from 4 to 45° in 2θ, with 0.008° steps and exposure time of 1.5 s for each step with stopping of the detector (about 3 h for each experiment). Rapid-scan experiments were conducted from 270 down to 100 K every 30 K, while high-resolution experiments were conducted at 100 and 210 K.

In all the patterns at low temperatures, peaks were found attributable to crystalline ice at 2θ angles higher than 18°, easily identified via Crystallographic and Crystallochemical Database for Minerals and their Structural Analogues, Institute of Experimental Mineralogy, Russian Academy of Sciences (website: http://database.iem.ac.ru/mincryst/index.php).

Table S1. Crystallographic and refinement data for Me_2btp, *t*Bu_2btp, **1a**·0.67DCM, **2a**·0.5Et_2O, **2b** and **4a**·4DCM.

	Me_2btp (100 K)	*t*Bu_2btp (120 K)	**1a**·0.67DCM (100 K)
Formula	$C_9H_9N_9$	$C_{15}H_{21}N_9$	$C_{18.67}H_{19.33}Cl_{9.33}Fe_3N_{18}$
M	243.25	327.41	994.27
T / K	100(2)	120(2)	100(2)
λ / Å	0.71073	Mo-Kα, 0.71073	Mo-Kα, 0.71073
Crystal system	monoclinic	monoclinic	monoclinic
Space group	$C2/c$	$P2_1/n$	$P2_1/n$
a / Å	14.286(4)	5.5931(3)	10.5339(11)
b / Å	6.6234(18)	29.6014(15)	41.199(4)
c / Å	11.245(3)	10.2101(5)	14.5213(15)
α/ °	90	90	90
β / °	99.228(8)	94.5168(19)	106.880(3)
γ/ °	90	90	90
Cell Volume/ Å^3	1050.3(5)	1685.17(15)	6030.6(11)
Z	4	4	6
D_C /Mg m^{-3}	1.538	1.290	1.643
μ / mm^{-1}	0.109	0.086	1.729
Dimensions / mm	0.16× 0.13× 0.12	0.40 × 0.07 × 0.07	0.21 × 0.16 × 0.10
$2\theta_{max}$,/º	54.0	52.2	50.1
Measured reflns	7128	13410	73435
Independent reflns	1147	3268	10675
R_{int}	0.0710	0.0580	0.0628
R_1, [$F^2>2\sigma(F^2)$]	0.0554	0.0744	0.1518
wR_2 [all data]	0.1313	0.1608	0.3678
S	1.056	1.125	1.118
Parameters, restraints	84, 0	223, 0	776, 866
$\Delta\rho_{max}$, $\Delta\rho_{min}$ / e Å^{-3}	0.287, –0.401	0.300, –0.313	2.966, –1.856
CCDC deposition number	2333079	2334366	2333080

Table S1 (cont.).

	2a·0.5Et_2O (293 K)	**2b** (100 K)	**4a**·4DCM (100 K)
Formula	$C_{32}H_{47}Cl_8Fe_3N_{18}O_{0.5}$	$C_{45}H_{65}Cl_8Fe_3N_{27}O$	$C_{34}H_{50}Cl_{10}FeN_{18}O_8$
M	1143.03	1451.39	1249.27
T, K	293(2)	100(2)	100(2)
λ, Å	0.71073	0.71073	0.71073
Crystal system	triclinic	trigonal	triclinic
Space group	$P\bar{1}$	$P3_121$	$P\bar{1}$
a / Å	15.3214(19)	11.6734(5)	13.379(15)
b / Å	16.879(2)	11.6734(5)	15.023(17)
c / Å	20.941(3)	41.617(2)	15.52(2)
α/ °	79.357(2)	90	98.75(2)
β / °	88.220(2)	90	113.730(14)
γ/ °	85.869(2)	120	90.077(16)
Cell Volume/ Å^3	5307.8(11)	4911.3(5)	2816(6)
Z	4	3	2
D_C/ Mg m^{-3}	1.430	1.472	1.474
μ / mm^{-1}	1.256	1.039	0.803
Dimensions / mm	0.22 × 0.13 × 0.11	016 × 0.15 × 0.11	0.16 × 0.11 × 0.08
$2\theta_{max}$ / º	52.0	54.0	50.0
Measured reflns	53786	69622	23687
Independent reflns	20703	7137	9854
R_{int}	0.0522	0.0465	0.1706
R_1 [$F^2>2\sigma(F^2)$]	0.0650	0.0391	0.1424
wR_2 [all data]	0.2307	0.0812	0.4103
S	1.006	1.176	1.043
Parameters, restraints	1245, 844	394, 1	641, 66
$\Delta\rho_{max}$, $\Delta\rho_{min}$ / e Å^{-3}	1.374, –0.547	0.0845, –0.500	1.398, –0.803
CCDC deposition number	2333109	2333081	2333082

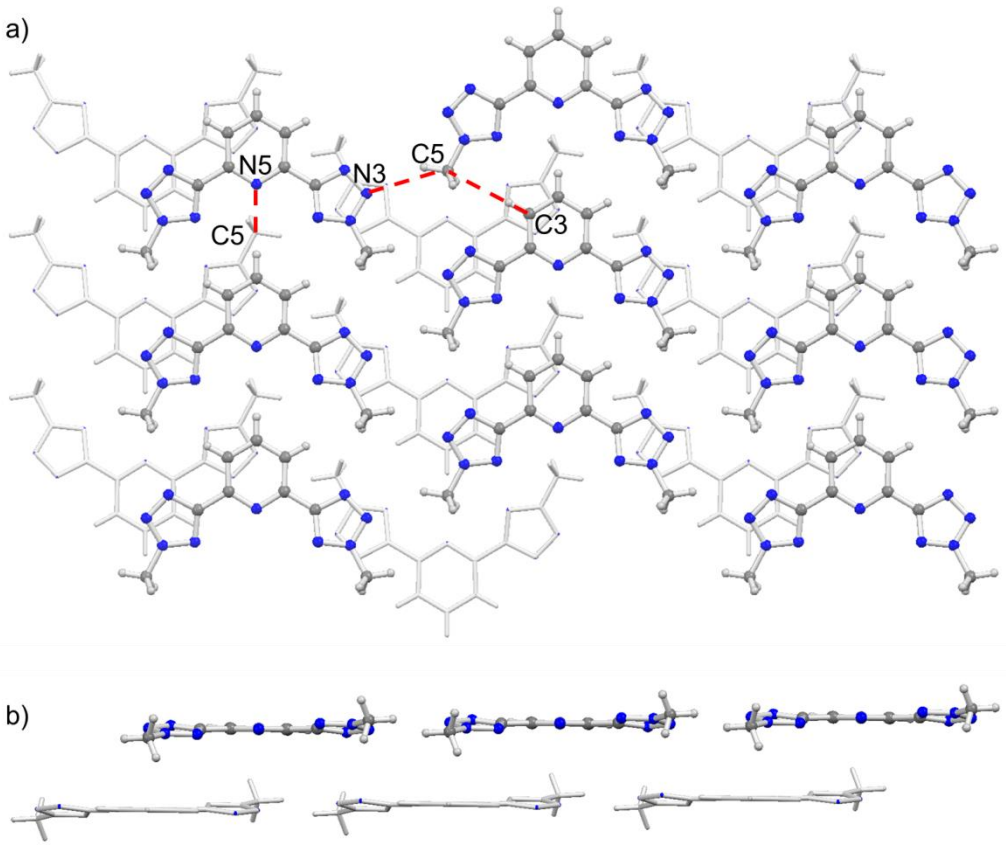

Figure S1. Crystal packing of Me_2btp a) perpendicular and b) along the crystallographic *b* axis; colour code: N = blue, C = grey, H = white, intermolecular contacts highlighted in dashed red lines.

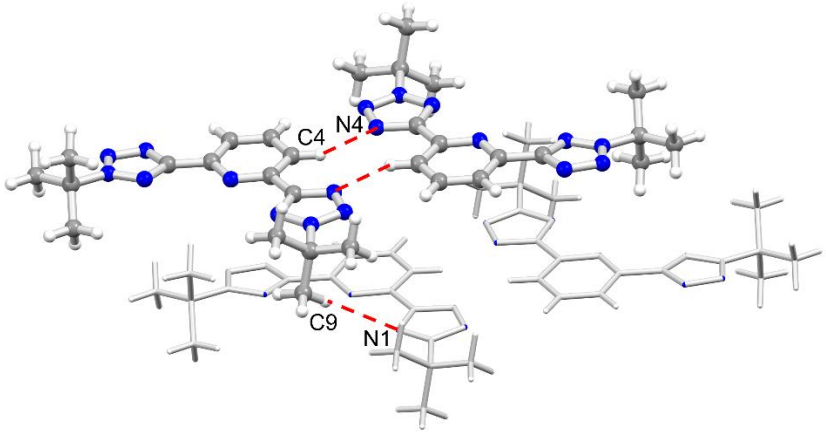

Figure S2. Crystal packing of *t*Bu_2btp; colour code: N = blue, C = grey, H = white, intermolecular contacts highlighted in dashed red lines.

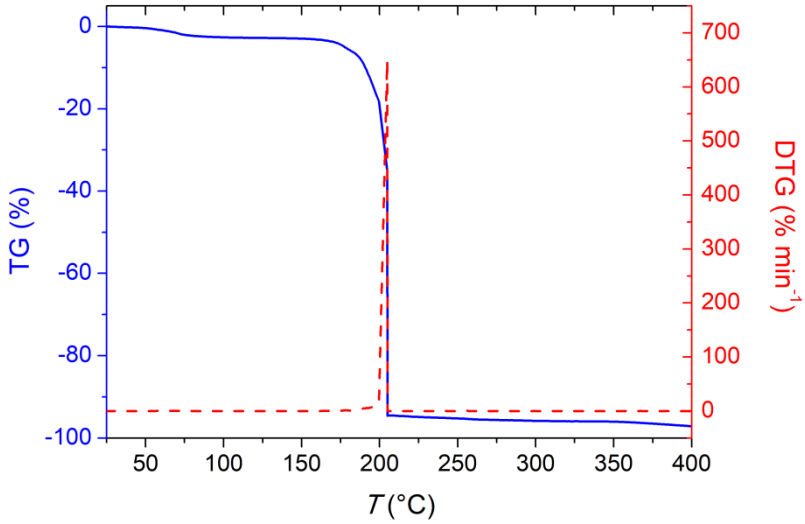

Figure S3. Thermogravimetric analysis of **4a**·1.5H_2O from room temperature up to 400 °C: TG signal (blue) together with its first derivative, DTG (red).

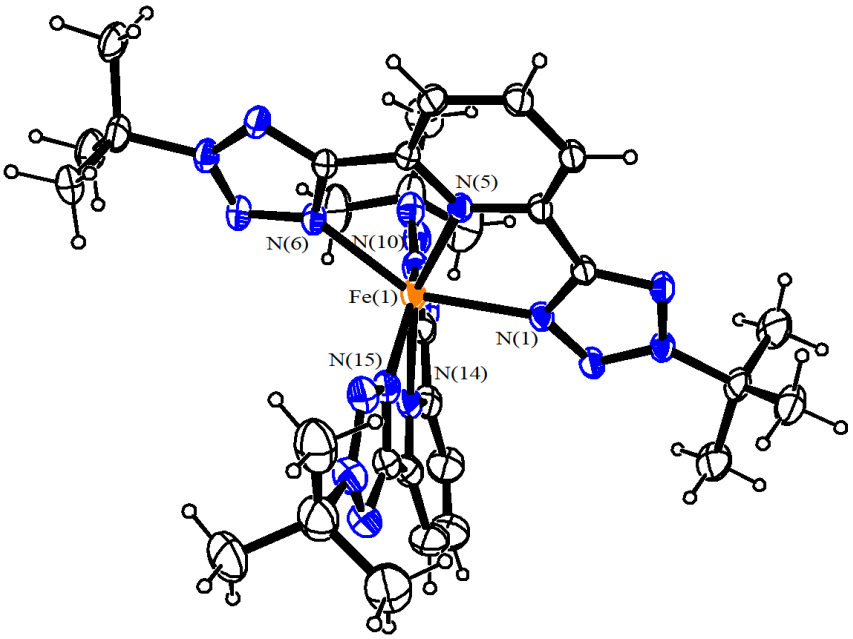

Figure S4. View of the molecular structure of the dication of **2a**·0.5Et_2O; displacement ellipsoids are at the 30% probability level; colour code: Fe = orange, N = blue, C and H = white; anions $FeCl_4^-$ and solvent molecules omitted for clarity.

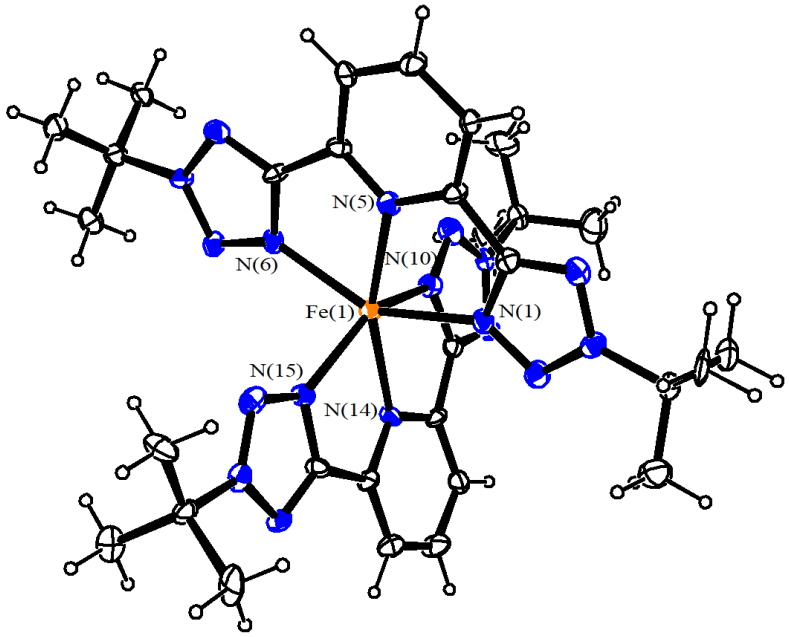

Figure S5. View of the molecular structure of the dication of **4a**·4DCM; displacement ellipsoids are at the 30% probability level; colour code: Fe = orange, N = blue, C and H = white; anions ClO_4^- and solvent molecules omitted for clarity.

Table S2. M06/6-311+G(d) coordination distances (Å) and angles (°), together with the distortion parameter θ (°), of $[Fe^{II}(Me_2btp)_2]^{2+}$ and $[Fe^{II}(tBu_2btp)_2]^{2+}$ dications in LS (S = 0) and HS (S = 2) states. For each parameter, the X-ray values of the corresponding $[Fe^{II}(R_2btp)_2](Fe^{III}Cl_4)_2$ (R = Me and *t*Bu) complexes in blue italics and of the corresponding $[Fe^{II}(R_2btp)_2](ClO_4)_2$ (R = Me and *t*Bu) in red italics are reported for direct comparison. Data for $[Fe^{II}(Me_2btp)_2](ClO_4)_2$ are adapted from the structural data of the co-crystal $[Fe(Me_2btp)_2][Fe(Me_2btp)(MeCN)_2(H_2O)](ClO_4)_4{\cdot}MeCN$ at 100 K.[8]

	$[Fe^{II}(Me_2btp)_2]^{2+}$		$[Fe^{II}(tBu_2btp)_2]^{2+}$	
	S = 0	S = 2	S = 0	S = 2
Fe(1)–N(1)	1.986	2.224	1.985	2.226
	1.950(11),1.947			*2.191(4),2.180(5)*
	1.946(3)			*2.227(13)*
Fe(1)–N(5) (py)	1.957	2.168	1.956	2.168
	1.928(10),1.937			*2.164(4),2.173(4)*
	1.924(3)			*2.184(12)*
Fe(1)–N(6)	1.986	2.192	1.985	2.186
	1.942(9),1.948			*2.147(4),2.195(4)*
	1.956(3)			*2.211(13)*
Fe(1)–N(10)	1.986	2.192	1.987	2.186
	1.934(11),1.930			*2.210(5),2.177(4)*
	1.947(3)			*2.268(14)*
Fe(1)–N(14) (py)	1.957	2.168	1.956	2.168
	1.926(11),1.940			*2.148(5),2.155(4)*
	1.925(3)			*2.196(12)*
Fe(1)–N(15)	1.984	2.224	1.984	2.226
	1.978(13),1.976			*2.206(6),2.180(5)*
	1.949(3)			*2.219(13)*
$r_{Fe–N\ (tetrazole)}$[a]	1.985	2.208	1.985	2.206
	1.951,1.950			*2.202,2.183*
	1.950			*2.231*
$r_{Fe–N\ (py)}$[a]	1.957	2.168	1.956	2.168
	1.927,1.938			*2.156,2.164*
	1.925			*2.190*
N(1)–Fe(1)–N(6) (ψ_1)	159.5	148.2	159.5	148.3
	160.1(5),159.3			*147.2(2),145.7(2)*
	160.76(12)			*148.4(5)*
N(10)–Fe(1)–N(15)(ψ_2)	159.6	148.2	159.5	148.3
	160.5(5),160.5			*146.8(2),147.4(2)*
	160.80(12)			*146.2(5)*
N(5)–Fe(1)–N(14) (ϕ)	179.8	164.2	179.6	161.0
	177.5(5), 177.7			*155.1(2),158.2(2)*
	177.07(12)			*161.7(5)*
θ[b]	90.00	83.98	90.00	84.44
	89.96			*80.47, 83.71*
	87.60			*85.10*

[a] Mean Fe–N distance; [b] Dihedral angle between the two ligands (the plane of each ligand was defined as the least-squares plane through its sixteen aromatic C/N atoms).

References

[1] G. M. Sheldrick, *Acta Crystallogr. Sect. C* **2015**, *71*, 3–8.

[2] A. L. Spek, *PLATON, A Multipurpose Crystallographic Tool*, Utrecht, The Netherlands, **2005**.

[3] Y. Zhao, D. G. Truhlar, *Theor. Chem. Acc.* **2008**, *120*, 215–241.

[4] Gaussian 16, Revision A.03, M. J. Frisch, G. W. Trucks, H. B. Schlegel, G. E. Scuseria, M. A. Robb, J. R. Cheeseman, G. Scalmani, V. Barone, G. A. Petersson, H. Nakatsuji, X. Li, M. Caricato, A. V. Marenich, J. Bloino, B. G. Janesko, R. Gomperts, B. Mennucci, H. P. Hratchian, J. V. Ortiz, A. F. Izmaylov, J. L. Sonnenberg, D. Williams-Young, F. Ding, F. Lipparini, F. Egidi, J. Goings, B. Peng, A. Petrone, T. Henderson, D. Ranasinghe, V. G. Zakrzewski, J. Gao, N. Rega, G. Zheng, W. Liang, M. Hada, M. Ehara, K. Toyota, R. Fukuda, J. Hasegawa, M. Ishida, T. Nakajima, Y. Honda, O. Kitao, H. Nakai, T. Vreven, K. Throssell, J. A. Montgomery, Jr., J. E. Peralta, F. Ogliaro, M. J. Bearpark, J. J. Heyd, E. N. Brothers, K. N. Kudin, V. N. Staroverov, T. A. Keith, R. Kobayashi, J. Normand, K. Raghavachari, A. P. Rendell, J. C. Burant, S. S. Iyengar, J. Tomasi, M. Cossi, J. M. Millam, M. Klene, C. Adamo, R. Cammi, J. W. Ochterski, R. L. Martin, K. Morokuma, O. Farkas, J. B. Foresman, and D. J. Fox, Gaussian, Inc., Wallingford CT, **2016**.

[5] M. Arczyński, J. Stanek, B. Sieklucka, K. R. Dunbar, D. Pinkowicz, *J. Am. Chem. Soc.* **2019**, *141*, 19067–19077.

[6] G. A. Bain, J. F. Berry, *J. Chem. Educ.* **2008**, *85*, 532–536.

[7] J. R. Plaisier, L. Nodari, L. Gigli, E. P. Rebollo San Miguel, R. Bertoncello, A. Lausi, *ACTA IMEKO* **2017**, *6*, 71.

[8] L. Rigamonti, L. Marchi, V. Fiorini, S. Stagni, S. Zacchini, D. Pinkowicz, K. Dziedzic-Kocurek, A. Forni, F. Muniz Miranda, R. Mazzoni, *Dalton Trans.* **2024**, *53*, 3490–3498.